GPO PRICE $ ______

CFSTI PRICE(S) $ ______

Hard copy (HC) 2.00

Microfiche (MF) .50

ff 653 July 65

CONVECTIVE HEAT TRANSFER IN A CONVERGENT-DIVERGENT NOZZLE[1]

L. H. Back[2]
P. F. Massier[3]
H. L. Gier[4]

N65-36564

JET PROPULSION LABORATORY
4800 Oak Grove Drive
Pasadena, Calif.

[redacted]

---

[1]Portions of this paper were originated under studies conducted for the Department of Army Ordnance Corps under Contract No. DA-04-495-Ord-18. Such studies are now conducted for the National Aeronautics and Space Administration under Contract No. NAS 7-100.

[2]Senior Research Engineer

[3]Research Group Supervisor

[4]Research Engineer

PREVIOUSLY
N65-36564 (ACCESSION NUMBER)
49 (PAGES)
CR 67025 (NASA CR OR TMX OR AD NUMBER)
1 (THRU)
(CODE)
33 (CATEGORY)
FACILITY FORM

ABSTRACT

The results of an experimental investigation of convective heat transfer from turbulent boundary layers accelerated under the influence of large pressure gradients in a cooled convergent-divergent nozzle are presented. The investigation covered a range of stagnation pressures from 30 to 250 psia, stagnation temperatures from 1030 to 2000°R, and nozzle-inlet boundary-layer thicknesses between 5 and 25% of the inlet radius. The most significant unexpected trend in the results is the reduction in the heat-transfer coefficient, below that typical of a turbulent boundary layer, at stagnation pressures less than about 75 psia. As expected, the results include a maximum in the heat-transfer coefficient upstream of the throat where the mass flow rate per unit area is largest, and a substantial decrease of the heat-transfer coefficient downstream of the point of flow separation which occurred in the divergent section of the nozzle at the low stagnation pressures. A reduction of about 10% in the heat-transfer coefficient resulted from an increase in the inlet boundary-layer thickness between the minimum and maximum thicknesses investigated.

Heat-transfer predictions with which the data were compared either incorporate a prediction of the boundary-layer characteristics or are related to pipe flow. At the higher stagnation pressures, predicted values from a modification of Bartz' turbulent-boundary-layer analysis are in fair agreement with the data. As a possible explanation of the low heat

transfer at the lower stagnation pressures, a parameter is found which is a measure of the importance of flow acceleration in reducing the turbulent transport below that typical of a fully turbulent boundary layer.

NOMENCLATURE

a	speed of sound
A	local nozzle cross-sectional area
A^*	nozzle throat area
c^*	characteristic velocity $p_o A^* g_c / \dot{m}$
c_f	local wall friction coefficient, $c_f/2 = \tau_w / \rho_e V_e^2$
c_f^*	coefficient analogous to skin-friction coefficient, with momentum thickness dependence replaced by energy thickness
c_p	specific heat at constant pressure
D	nozzle diameter
D^*	nozzle throat diameter
g_c	gravitational constant
h	convective heat-transfer coefficient
l	cooled-approach length
L	axial length of nozzle = 5.925 in.
$\dot{m}$	mass flow rate
M	Mach number
p	static pressure
p_t	stagnation pressure
Pr	Prandtl number
q_w	wall heat flux
$q^2/2$	turbulent kinetic energy
r	nozzle radius

NOMENCLATURE (Cont'd)

r^*	nozzle-throat radius
r_c	nozzle-throat radius of curvature
t	nozzle-inlet radius = 2.53 in.
Re_D	Reynolds number based on nozzle diameter, $\rho_e V_e D/\mu_e$
St	Stanton number, $h/\rho_e V_e c_p$
T	temperature
u	velocity component in axial direction
v	velocity component normal to wall
V_n	velocity component normal to nozzle centerline
V_e	velocity parallel to nozzle wall at outer edge of boundary layer.
x	axial distance from nozzle inlet
y	distance normal to wall
γ	specific-heat ratio
δ	velocity boundary layer thickness
δ_t	stagnation-temperature boundary-layer thickness
δ^*	displacement thickness
θ	momentum thickness
μ	viscosity
ν	kinematic viscosity
ρ	density
σ	dimensionless property correction factor (defined in Ref. 17)

NOMENCLATURE (Cont'd)

τ_w	wall shear stress
ϕ	energy thickness
χ	parameter

Subscripts

aw	adiabatic wall condition
e	condition at free-stream edge of boundary layer
f	property evaluated at film temperature, $T_f = T_w + T_e/2$
i, j	components in Cartesian coordinates
o	upstream reservoir condition
t	stagnation condition
w	wall condition
1	one-dimensional flow value

Superscripts

$(\ )'$	fluctuating component
$\overline{(\ )}$	time average

INTRODUCTION

Comprehensive studies of convective heat transfer from gases flowing under the influence of comparatively large pressure gradients have been mostly analytical. Laminar-flow cases have been solved by boundary-layer theory approaches in which the restrictive assumptions are within the realm of describing actual processes. Turbulent flows, however, are too complex to formulate in such a way that descriptions of the momentum and energy transport processes can be made without the use of considerable empirical information or assumptions which are so drastic that they themselves are essentially the solutions. The present investigation was undertaken in order to provide experimental convective heat-transfer information on turbulent flows subjected to large pressure gradients with boundary layers that are thin in comparison to the cross section of the channels. It was anticipated that these results could be incorporated with turbulent boundary-layer theories to arrive at a meaningful method of predicting convective heat transfer in accelerating flows.

Experimental measurements of heat transfer from gases flowing under the influence of pressure gradients have been made to some extent by other investigators. Data obtained from rocket-engine firings indicate that the local heat fluxes in nozzles (particularly the convergent sections) are sensitive to injection schemes, combustion phenomena, and the proximity of a nozzle to the injector [1]. Furthermore, superimposed on the convective component is a radiation component which, together with the other effects, introduces complexities into the gross heat-transfer process. Hence, results of measurements such as these have not been particularly informative about the convective heat-transfer mechanism in accelerating turbulent boundary-layer flows.

Experimental results of previous investigations of convective heat transfer in a nozzle in which injection and combustion effects were absent are scarce. Saunders and Calder's measurements [2] were made only in the conical divergence section of a nozzle with the half-angle of divergence about 1/2 deg. Kolozsi [3] reported measurements at only two operating conditions in a 7 1/2-deg half-angle convergent and divergent conical nozzle. The stagnation temperature was about 1200°R, and the stagnation pressures were 225 and 370 psia. Ragsdale and Smith [4], using superheated steam, made measurements in a nozzle which has small convergent and divergent half-angles of about 1 deg. The stagnation temperature was about 1000°R, and the stagnation pressure ranged from 20 to 35 psia. In preliminary results [5] from the system shown in Fig. 1, semilocal values of heat transfer were determined by calorimetry for a few operating conditions.

In this investigation, compressed air was heated by the internal combustion of methanol and then mixed to obtain uniformity before it entered the nozzle. The mixing and distance of the combustion from the nozzle (Fig. 1) minimized maldistributions. The nozzle had a throat diameter of 1.803 in., a contraction-area ratio of 7.75 to 1, an expansion-area ratio of 2.68 to 1 a convergent half-angle of 30 deg, and a divergent half-angle of 15 deg. The exit Mach number was about 2.5. Local convective heat-transfer results were obtained by measuring steady-state temperatures with thermocouples embedded in the water-cooled nozzle wall. Radiation effects were negligible over the 1030 and 2000°R stagnation-temperature range. To determine the effect of boundary-layer thickness at the nozzle inlet on heat transfer in the nozzle, the length of the constant-diameter cooled-approach section upstream of the nozzle inlet was changed in 6-in. lengths from 0 to 18 in.

INSTRUMENTATION AND HEAT-TRANSFER CALCULATION PROCEDURE

The system flow and instrumentation diagram is shown in Fig. 1. The ratio of methanol-to-air weight flow rate was small enough, even for the highest stagnation temperature, so that the products of combustion could be treated approximately as air. Stagnation pressure was measured just upstream of the water-cooled approach section, and stagnation temperature was determined by averaging the readings of two shielded thermocouples located 0.25 in. upstream of the nozzle inlet. These two thermocouples, located 1 in. from the centerline, were spaced 180 deg apart circumferentially and generally read within 2% of each other. To determine the static-pressure distribution along the nozzle, thirty-two static-pressure holes 0.040 in. in diameter were spaced circumferentially and axially in the nozzle wall. These static pressures were measured with mercury manometers.

Boundary-layer traverses were made in the 5.06-in.-diameter cooled-approach section at a location 1.25 in. upstream of the nozzle inlet. The stagnation-pressure probe was located 90 deg circumferentially from the stagnation-temperature probe. Details of the probe tips are shown in Fig. 2. The tip design is similar to that of probes used by Livesey [6], with which he found a negligible velocity displacement effect of the probe in the wall vicinity.

The thermocouples embedded in the wall of the nozzle were first assembled by percussion-welding the exposed ends of 0.005-in.-diameter fiberglass-insulated chromel and alumel thermocouple wires to the bottoms of holes drilled radially into cylindrical plugs, as shown in Fig. 3. These plugs, made from the same billet of 502-type stainless steel used to fabricate the nozzle, were pressed into holes drilled through the nozzle wall. Three thermocouples were formed along the length of each plug. One thermocouple plug was located at each of twenty-one axial locations, except at $x/L = 0.864$ where there were two. The thermocouple plugs were also spaced at numerous circumferential locations along the nozzle, as indicated in the table in Fig. 3, such that every third plug was located in a quadrant within 55 deg of successive ones. A technique for electrically determining the location of the thermocouple weld junctions was devised using a Kelvin bridge circuit. Three longitudinal water-coolant passages were used to cool the outer surface of the nozzle and plugs.

Although temperature gradients existed along the nozzle wall, these were generally small, and the three thermocouple readings in each plug indicated that only radial heat conduction normal to the wall need be considered. The gas-side wall temperatures determined from the different thermocouple combinations in each plug were generally within 1%. However, in determining the wall heat flux, there were inconsistencies. If the center thermocouple and the one nearest the gas-side wall were used, the calculated wall heat flux was on the average about 10% higher than when the thermocouples nearest the gas-side and water-side walls were used. With a combination of the center thermocouple and the one nearest the gas-side wall, the total heat load was found to agree within 5% of that computed from the coolant flow rate and the coolant temperature rise; consequently, these two thermocouples were used to calculate the wall heat flux.

The heat-transfer coefficient was computed by

$$h = \frac{q_w}{T_{aw} - T_w}$$

In the absence of adiabatic wall measurements in nozzles, the adiabatic wall temperature was calculated by assuming a recovery factor of 0.89.

STATIC PRESSURE AND MASS FLUX DISTRIBUTIONS

The measured static-to-stagnation pressure ratio along the nozzle is shown in Fig. 4 at a stagnation temperature of 1500°R for a range of stagnation pressures from 45 to 150 psia. Measurements at higher stagnation pressures were not possible because of manometer limitations. Except in the nozzle-exit region, where the rapid rise in static pressure at the lower stagnation pressures indicates flow separation, the pressure-ratio distribution is nearly invariant. For computational purposes, it is assumed to be invariant above 150 psia. Deviations of measured pressure distributions from that predicted from one-dimensional isentropic flow are indicated. Just downstream of the throat, these amount to 30%. The deviations result from radial-velocity components caused by the taper and curvature of the nozzle.

In Fig. 5, the ratio of the local mass flux $\rho_e V_e$, calculated from the measured wall static pressures, to that predicted from one-dimensional flow $\rho_1 u_1$, is shown at $p_t = 75$ psia for different stagnation temperatures and cooled-approach lengths. For the tests shown, the maximum value of the mass flux $\rho_e V_e$ occurred at $x/L = 0.58$. This location corresponds to the intersection of the sonic line with the nozzle wall and is upstream of the geometric throat, which is located at $x/L = 0.603$. Just downstream of the throat, there is a sharp dip in the mass-flux ratio, the reduction below that predicted from one-dimensional flow amounting to about 15%. There appears to be a slight trend toward mass-flux ratios increasing with stagnation temperature, especially near the nozzle exit. The effect of boundary-layer thickness at the nozzle inlet on the mass-flux ratio is negligible.

Since the deviations from one-dimensional flow are significant in the throat region, it is of interest to determine to what extent the mass flux at the edge of the boundary layer is predictable. Oswatitsch and Rothstein [7] considered isentropic, two-dimensional flow in a converging-diverging nozzle. The wall boundary layer is neglected as is the requirement that the fluid velocity at the wall be exactly parallel to it. The final result of their analysis can be cast in the form of a ratio of the mass flux at the nozzle wall to that for one-dimensional flow

$$\frac{\rho_e V_e}{\rho_1 u_1} = \frac{\left\{ 1 - \frac{\gamma - 1}{2} \left(M_1 \frac{a_1}{a_0} \right)^2 \left(\frac{V_e}{u_1} \right)^2 \right\}^{\frac{1}{\gamma - 1}}}{\frac{\rho_1}{\rho_0}} \left(\frac{V_e}{u_1} \right) \tag{1}$$

where:

$$\frac{V_e}{u_1} = \sqrt{\left(\frac{u_e}{u_1} \right)^2 + \left(\frac{v_{ne}}{u_1} \right)^2}$$

$$= \sqrt{\left\{ 1 + \frac{1}{2} \left[\frac{1}{2} r \frac{d^2 r}{dx^2} + \frac{1}{4} \frac{du_1/dx}{u_1} r \frac{dr}{dx} - \left(\frac{dr}{dx} \right)^2 \right] \right\}^2 + \left(\frac{dr}{dx} \right)^2}$$

The predicted mass-flux ratio is only a function of the nozzle geometry, with the subscript 1 denoting average quantities for one-dimensional flow. The prediction shown in Fig. 5 is in fair agreement with the data in the throat region. It also indicates the sonic line to be upstream of the throat. At the intersection of the conical sections of the nozzle with the throat curvature, there is a predicted discontinuity in the mass-flux ratio as indicated by the dashed lines. The prediction is not shown in the nozzle-entrance region since there, restrictions on the magnitude of the nozzle radius and its derivations implied in the analysis are not satisfied. Even in the throat region, these are marginal.

BOUNDARY LAYERS AT THE NOZZLE INLET

To indicate the nature of the boundary layer at the nozzle inlet with the 1[illegible]-in. cooled-approach length, the velocity ratio u/u_e, mass-flux ratio $\rho u/\rho_e u_e$, and stagnation-temperature distribution $(T_t - T_w)/(T_{te} - T_w)$ are shown in Fig. 6 for a stagnation temperature of 1500°R and a range of stagnation pressures from 45 to 254 psia. The profiles indicate that the boundary layers are turbulent over the range of stagnation pressures. A 1/7-power-law curve for negligible property variation across the boundary layer is shown for comparison. Values of the thicknesses δ^*, θ, and ϕ near the nozzle inlet were calculated by taking into account the mass, momentum, and energy defects for flow through a pipe of radius R. For example, the momentum thickness was calculated from

$$\theta\left(R - \frac{\theta}{2}\right) = \int_0^{\delta} \frac{\rho u}{\rho_e u_e}\left(1 - \frac{u}{u_e}\right)\left(R - y\right)dy$$

In general, these thicknesses are about 5% lower than those obtained by assuming flow over a plane surface. The effect of increasing stagnation pressures is to decrease the displacement, momentum, and energy thicknesses.

At the other stagnation temperatures of 1030 and 2000°R, as well as with the shorter cooled-approach lengths of 6 and 12 in., the boundary-layer profiles, though not shown, were also turbulent. However, with no cooled-approach length, the boundary layer appears to be in the transition region, as indicated by the velocity profiles shown in Fig. 7. These profiles lie between a turbulent and laminar one, as shown by the 1/7-power law and Blasius laminar-flow profiles.

HEAT-TRANSFER RESULTS

The variation of the heat-transfer coefficient along the nozzle with the 18-in. cooled-approach length is shown in Fig. 8 for stagnation temperatures of about 1030, 1500, and 2000°R and a range of stagnation pressures from 30 to 254 psia. At the highest stagnation temperature, it was not possible to obtain data above a stagnation pressure of 125 psia because of temperature limitations on the wall-thermocouple insulating material. The curves in the Figure were faired through the data. It is evident that during a given test, circumferential variations in heat transfer did exist, as indicated by the symbols which are tagged in the same manner. These indicate thermocouple plugs spaced within 55 deg of each other. A certain amount of consistency can be deduced by comparing data obtained from the same thermocouple plugs for different tests. The majority of the tests were duplicated and found reproducible to within about ±2%. It was not

To represent the heat-transfer results shown in Fig. 8 in terms of correlation parameters commonly used involves both the selection of a characteristic length and the temperature at which properties are evaluated. In Fig. 9 there are shown, in addition to the data of Fig. 8, data from many more tests at intermediate stagnation pressures presented in terms of the group, St $Pr^{0.6}$, and the Reynolds number based on the local nozzle diameter. Fluid properties were evaluated at the static temperature at the edge of the boundary layer, and the mass flux $\rho_e V_e$ was used to compute both the Stanton and Reynolds numbers. Each of the plots in Fig. 9 indicates the heat-transfer data obtained at a single area ratio or axial station. Hence, in each of the plots, increasing Reynolds numbers $\rho_e V_e D/\mu_e$ at the different stagnation temperatures correspond directly to increasing stagnation pressures, since the nozzle diameter is constant.

Proceeding through the subsonic part of the nozzle (decreasing area ratios), there is a substantial reduction in heat transfer at the lower stagnation pressures below that typical of a turbulent boundary layer, where the dependence of the heat-transfer coefficient on the mass flux is $h \alpha (\rho_e V_e)^{4/5}$. This reduction persists through the throat and into the supersonic region before it diminishes near the nozzle exit. At the higher stagnation pressures, above 75 psia, the heat transfer is typical of a turbulent boundary layer.

Other investigators have observed unexpected trends accompanying the acceleration of turbulent boundary layers. The trends shown in Fig. 9

possible to explain these variations by nonuniformities in the flow based on measurements in the gas stream at the nozzle inlet. However, it is possible that nonuniformities could have existed in the boundary layer.

The heat-transfer results shown in Fig. 8 indicate the following:

1. The heat-transfer coefficients increase with increasing stagnation pressures as a result of larger mass fluxes.

2. The variation of the heat-transfer coefficients with stagnation temperature at the different stagnation pressures is less clear, with the trends dependent on stagnation pressure.

3. The maximum value of the heat-transfer coefficients occurs just upstream of the throat in the vicinity where the mass flux $\rho_e V_e$, as indicated in Fig. 5, is a maximum.

4. A substantial decrease in heat transfer downstream of the point of flow separation which occurred at the low stagnation pressures is indicated by the tests at a stagnation pressure of 45 psia. At the lowest stagnation pressure, the data are not shown in this region, since there were large fluctuations in the wall-thermocouple readings.

are similar to the results of Ref [1] which were obtained from rocket-engine tests over a similar range of stagnation pressures. The large positive slope of the experimental curves at area ratios near one was noted as well as the eventual decrease in slope with increasing stagnation pressure. This implies that for the rocket-engine tests, injection and combustion effects did not substantially alter the heat-transfer trends from those indicated in Fig. 9. In Ref. [8], a turbulent boundary layer at the entrance of a supersonic nozzle was found to undergo transition to a nearly laminar one at the nozzle exit. The stagnation pressure was 4.3 psia. When the stagnation pressure was increased to 14.2 psia, a turbulent boundary layer was found at the nozzle exit. No boundary layer measurements were made within the nozzle. In Ref. [9], it was observed that heat-transfer trends of the type seen here at the low stagnation pressures existed under lower pressure-gradient conditions. For momentum thickness Reynolds numbers $\rho_e V_e \theta/\mu$, less than about 600, there was departure from fully turbulent flow through the acceleration region as indicated by the linearity of the measured velocity profiles in the wall vicinity.

From these observations it seems logical to speculate that at the lower stagnation pressures, the boundary layer may have undergone transition from the turbulent profile at the nozzle inlet to a partially laminar profile under the influence of the large, favorable pressure gradient. The consequent decrease in eddy transport would reduce both the wall friction and heat transfer. In the last Section, a parameter relating a predicted reduction in net production of turbulent kinetic energy to the low stagnation pressures is discussed.

The effect of varying nozzle-inlet boundary-layer thicknesses on the heat transfer is shown in Fig. 10, in particular for a stagnation temperature of 1500°R and a range of stagnation pressures from 75 to 200 psia. With no cooled-approach length, for which the ratio of estimated boundary-layer thickness to nozzle-inlet radius is about 0.05, the heat-transfer coefficient is above the thicker layer results. This trend persists through the nozzle and extends into the supersonic region. Just upstream of the throat, where the heat transfer coefficient is a maximum, the thinnest layer results exceed the thickest layer results obtained with the 18-in. cooled-approach length by about 10%. Apparently, with no cooled-approach length, transition from the boundary-layer profile shown in Fig. 7 to a turbulent one occurred upstream of the first heat-transfer measuring station.

COMPARISON OF HEAT-TRANSFER RESULTS WITH PREDICTIONS

The methods of predicting heat transfer that will be compared with test results are those involving a knowledge of the boundary layer: (1) a modification of the turbulent boundary-layer analysis of Ref. [10], (2) the von Kármán analogy (Eq. 3) and those related to pipe flow, (3) the pipe-flow equation (Eq. 4), and (4) Bartz' simplified equation (Eq. 5). A complete report on the computation procedure of the modified boundary-layer analysis, which is programmed for numerical solution on an I. B. M. 7090 computer, is presented in Ref. [11].

Before discussing the boundary-layer-type predictions, mention should be made of the uncertainty as to whether or not a form of Reynolds analogy between heat transfer and wall friction is valid in nozzle heat transfer. A limited amount of data [9, 12, 13] for heat transfer to an accelerated, essentially incompressible, turbulent boundary layer where property variations were small has indicated that heat-transfer coefficients determined from the wall friction through one of the analogies known to apply for constant free-stream velocity were far in excess of actual values. However, since boundary-layer measurements were not made in the nozzle, a direct experimental check at this point was not possible.

The heat-transfer specification from the modified turbulent boundary-layer analysis [11] is

$$\frac{h}{\rho_e V_e c_p} = K^* \frac{c_f^*}{2} \left(\frac{\phi}{\theta}\right)^n \qquad (2)$$

where

$$K^* = \left\{ \sqrt{\frac{c_f^*}{2}} \left[5 \text{ Pr} + 5 \ln(5 \text{ Pr} + 1) - 14 + \sqrt{\frac{2}{c_f^*}} \right] \right\}^{-1}$$

The momentum and energy equations are solved to determine ϕ and θ. The factor K^* is similar to the Prandtl-number correction factor in the von Kármán analogy. The coefficient c_f^* is analogous to the wall friction coefficient c_f but with the momentum thickness dependence replaced by the energy thickness. The ratio $(\phi/\theta)^n$ is used to correct partially for a hydrodynamic dependence. The wall friction coefficient is predicted either from the Blasius flat-plate relation with properties ρ and μ evaluated at the film temperature, as was done in the earlier analysis [10], or by taking the adiabatic wall friction coefficient [predicted from Cole's relation [14] between the friction coefficient for a compressible and incompressible flow] with properties evaluated at the free-stream temperature. This latter method is suggested by a limited amount of data [15] which indicate both the Stanton number and wall friction coefficient with properties evaluated at the free-stream temperature to be insensitive to severe wall cooling. Of note is that for a severely cooled wall, the friction coefficient predicted by the latter method is substantially below that predicted by evaluating properties at the film temperature.

To predict the heat-transfer coefficient from Eq. (2) requires the selection of n and the temperature at which properties are to be evaluated. With $n \simeq 0.1$, the prediction is approximately the same as that of Ref. [10]. For comparison purposes, however, it seems appropriate to consider the two limiting values of n. These correspond to assuming a Stanton-number dependence only on the thermal characteristic ϕ; i.e., $n = 0$, for which Eq. (2) becomes

$$\frac{\quad}{\rho_e V_e}\,\frac{\quad}{c_p} = K^* \frac{c_f^*}{2} \qquad \text{(2a)}$$

or to taking n = 0.25, for which Eq. (2a) becomes approximately the von Kármán analogy

$$\frac{h}{\rho_e u_e c_p} = K \frac{c_f}{2} \tag{3}$$

where

$$K = \left\{ \sqrt{\frac{c_f}{2}} \left[5\,\mathrm{Pr} + 5 \ln(5\,\mathrm{Pr} + 1) - 14 + \sqrt{\frac{2}{c_f}} \right] \right\}^{-1}$$

Other analyses which assume a Stanton-number dependence only on ϕ have been made in Refs. [12] and [16] and compared to experimental heat-transfer results for accelerated turbulent boundary-layer flows. In Ref. [12], the predictions exceeded the data by about 30% in part of the acceleration region, while in Ref. [16], the correspondence with the data was good.

The heat-transfer predictions shown in Fig. 11 as curve A are from Eq. (2a) for a stagnation temperature of 1500°R and a range of stagnation pressures from 45 to 254 psia, with the 18-in. cooled-approach length. These predictions were made with properties evaluated at the free-stream temperature and conditions at the edge of the boundary layer determined from the wall static-pressure measurements. Shown as curve C in Fig. 11 is the prediction from Eq. (3), in which the friction coefficient $c_f/2$ was determined from the modified turbulent boundary-layer analysis. The reduction in the predicted heat-transfer coefficients provided by Eq. (2a) below the von Kármán analogy is due to the thicker predicted thermal than velocity boundary-layer thicknesses through the nozzle. At the highest stagnation pressure, the predicted ratios of ϕ/θ as indicated in Fig. 12 are as large as 5 in the throat region. At the 75-psia stagnation pressure, the correspondence of the prediction from the modified turbulent boundary-layer analysis Eq. (2a) with the data is good except near the nozzle exit. At the highest stagnation pressure of 254 psia, where the circumferential variation of the data is considerable, the correspondence with the averaged heat-transfer data is fair. The reproducibility of the data in Fig. 11 for 254 psia is indicated by the two sets of data shown by the open and shaded symbols. At the lowest stagnation pressure, p_t = 44.8 psia, the prediction exceeds the data by as much as 50% in the throat region. For the range of stagnation pressures, the predicted maximum value of the heat-transfer coefficient is just upstream of the throat, in agreement with the data.

The effect of temperature choice for property evaluation may be observed in Fig. 11 by comparing curves A and B. Curve B represents Eq. (2a) with properties evaluated at the film temperature T_f. In the throat region, it lies above the data.

For comparison purposes, the predictions from the following form of the pipe-flow equation for fully developed flow in which both the thermal and velocity boundary layer extend to the centerline and in which there is no significant pressure gradient are shown as curve D in Fig. 11.

$$St \, Pr^{0.6} = 0.023 \, Re_D^{-0.2} \tag{4}$$

Also shown as curve E in Fig. 11 is the equation of Ref. 17.

$$h = \left[\frac{0.026}{(D^*)^{0.2}} \left(\frac{\mu^{0.2} c_p}{Pr^{0.6}} \right)_o \left(\frac{p_o g_c}{c^*} \right)^{0.8} \left(\frac{D^*}{r_c} \right)^{0.1} \right] \left(\frac{A^*}{A} \right)^{0.9} \sigma \tag{5}$$

In the pipe-flow equation, all properties were evaluated at the free-stream static temperature, while in Eq. (5), the Prandtl number and specific heat were assumed constant at their stagnation temperature values and ρ and μ were evaluated at the film temperature. In Eq. (5), one-dimensional flow quantities were used, since two-dimensional effects are not taken into account in the derivation. If they were, the prediction would be nearer that of the pipe-flow equation. Two-dimensional values of local mass flux are 15% below the one-dimensional values just downstream of the nozzle throat, as seen in Fig. 6. The prediction from Eq. (5) exceeds the data by as much as 80% in the throat region. The pipe-flow equation (Eq. 4) prediction, though in better agreement with the data, is still about 25% high at the throat.

From these observations, it appears that fair agreement with the data is provided at the higher stagnation pressures by the modified boundary-layer analysis taken in the form of Eq. (2a), with properties evaluated at the free-stream static temperature. These predictions are also shown, along with others, at the intermediate pressures of p_t = 60 and 150 psia for T_{to} = 1500°F as curve A in Fig. 9. The predicted Stanton-number dependence on the mass flux is approximately that of the pipe-flow equation, which is shown as curve D. However, an approximation cannot be made of the prediction for all the axial locations by an equation like the pipe-flow equation but with a lower coefficient. This is due to the variation of the predicted value of ϕ relative to D. For a given run, ϕ decreases through the subsonic region, attaining a minimum near the throat, and then increases in the supersonic region, qualitatively similar but not in direct correspondence with the nozzle diameter. A few of these predicted ratios are shown in Fig. 12.

In Figs. 9c through 9i, the reduction in heat transfer at Reynolds numbers Re_D less than about 8×10^5 is not predictable from an analysis for a turbulent boundary layer, as indicated by the prediction from Eq. (2a) shown in Fig. 9 as curve A.

Predictions from Eq. (2a) were also made, though not shown, at stagnation temperatures of 1030 and 2000°R, with the 18-in. cooled-approach length. The magnitude of the decrease in the heat-transfer coefficient with increasing stagnation temperature at the higher stagnation pressures shown in Fig. 8 was not predictable. From Eq. (2a), the dependence of the heat-transfer coefficient on stagnation temperature at a given stagnation pressure is nearly $h \propto T_{to}^{-0.28} \phi^{-0.2}$. However, the energy thickness at the nozzle inlet decreased with increasing stagnation temperature, such that the difference in predicted heat-transfer coefficients was substantially less than exhibited by the data.

The trend of higher heat transfer coefficients through the nozzle with thinner boundary layers at the nozzle inlet is shown in Fig. 10 to be predictable from Eq. (2a). However, the magnitude of the predicted increase should probably be estimated from the 6- and 18-in. cooled-approach length predictions. For the zero cooled-approach length prediction, wall cooling was assumed to begin at the nozzle inlet and to require that the Stanton numbers remain finite there; the energy thickness was taken at a small value equal to 0.001 in.

SOME ADDITIONAL OBSERVATIONS OF THE FLOW AND THERMAL CHARACTERISTICS

In this Section, some features of the flow are shown which depend on the predicted flow and thermal characteristics obtained from the modified turbulent boundary-layer analysis [11], with properties evaluated at the free-stream temperature. In Fig. 12, the predicted ratios of ϕ/θ and δ_{ϕ}/δ indicate the thicker predicted thermal than velocity boundary layers, especially in the throat region. Because of the cooled wall, the displacement thickness δ^* becomes negative upstream of the throat, as does $H = \delta^*/\theta$.

In Fig. 13, the predicted momentum thickness Reynolds numbers are at a minimum a considerable distance upstream of the throat. At the lowest stagnation pressure, where the heat transfer is below that typical of a turbulent boundary layer, the minimum Reynolds number is 1500.

Although this predicted value is probably different from the actual value, it is still considerably above the measured value of 600 found in Ref. [9]. For the case of constant free-stream velocity, Preston [18] proposed a value of 320, above which the flow could be considered fully turbulent; for accelerated flows, he estimated that the limit might be lower.

To indicate the magnitude of the forces acting on the boundary layer through the nozzle, the ratio of the pressure forces which tend to accelerate the boundary-layer flow to the retardation wall shear forces is shown in Fig. 14 as

$$- \frac{\delta \frac{dp}{dx}}{\tau_w}$$

The ratio is largest in the convergent section before decreasing through the throat and divergent section. For comparison, the value of the ratio for fully developed flow in a circular pipe is shown to demonstrate the large flow accelerations in a nozzle.

To gain some knowledge of the mechanism which at the low stagnation pressures reduces the heat transfer below that typical of a fully turbulent boundary layer, reference is made to the turbulence-energy equation (e.g., see [19]). For simplicity, an incompressible flow is assumed* for which the convection of turbulent kinetic energy by the mean flow is

---

*It can be shown that the terms in Eq. (7) are the same for an incompressible axisymmetric turbulent boundary-layer flow, where the coordinates are taken along the surface and the boundary layer is thin.

$$u_j \frac{\partial \overline{q^2/2}}{\partial x_j} = - \overline{u_i' u_j'} \frac{\partial u_i}{\partial x_j} - \frac{\partial}{\partial x_j} \overline{u_j' \left(\frac{p'}{\rho} + \frac{q^2}{2} \right)} + \nu \overline{u_i' \frac{\partial^2 u_i'}{\partial x_j^2}} \tag{6}$$

(a) (b) (c) (d)

The terms represent the following:

(a) production of turbulent kinetic energy by the working of the mean velocity gradients against the Reynolds stresses

(b) work done by the turbulence against the fluctuation pressure gradients

(c) convection of turbulent kinetic energy by the turbulence itself

(d) transfer of energy by the working of the turbulent viscous stresses

In a pressure-gradient flow, the significant terms from term (a) that lead to a production or decay of convected turbulent kinetic energy are

$$- \overline{u_i' u_j'} \frac{\partial u_i}{\partial x_j} = - \overline{u'v'} \frac{\partial u}{\partial y} - \overline{(u')^2} \frac{\partial u}{\partial x} \tag{7}$$

The remaining terms in Eq. (6) adopt values consistent with the production terms. The first term in Eq. (7) is always positive and leads to a production of turbulent kinetic energy. However, with flow acceleration $\partial u/\partial x > 0$, the second term leads to a decay of turbulent kinetic energy. Thus, a measure of the importance of flow acceleration in reducing the net production of turbulent kinetic energy is given by a ratio of the two terms in Eq. (7):

$$\chi = \frac{\overline{(u')^2}\,\frac{\partial u}{\partial x}}{-\overline{u'v'}\,\frac{\partial u}{\partial y}} \tag{8}$$

To establish the variation of χ in the flow direction requires a knowledge of the turbulent quantities across the boundary layer. In the absence of turbulence measurements in accelerated flows, this estimate is restricted to the flat-plate measurements of Klebenoff [20] at a momentum thickness Reynolds number of about 8×10^3. The production term $-\overline{u'v'}\ \partial u/\partial y$ is largest in the wall vicinity where $\left(y\sqrt{\tau_w/\rho_e}\right)/\nu_e \simeq 30$. Using the "law of the wall,"

$$\frac{u}{\sqrt{\frac{\tau_w}{\rho_e}}} = 5.5 + 2.5\ \ln \frac{y\sqrt{\frac{\tau_w}{\rho_e}}}{\nu_e}$$

the velocity gradient is

$$\frac{\partial u}{\partial y} = \frac{2.5}{30}\,\frac{\tau_w}{\rho_e \nu_e}$$

The ratio $\overline{q^2}/-\overline{u'v'}$ was found to be relatively constant across most of the boundary layer. Relating $\overline{(u')^2}$ to $\overline{q^2}$ at half the boundary-layer thickness gives $\overline{(u')^2}/-\overline{u'v'} \simeq 3$. Approximating the velocity gradient $\partial u/\partial x$ by its free-stream value du_e/dx and combining the other approximations gives

$$\chi = \frac{36\,\nu_e \dfrac{du_e}{dx}}{\dfrac{\tau_w}{\rho_e}}$$

Although the constant, 36, is somewhat arbitrary, the essential feature is the dependence of χ on the group,

$$\frac{\nu_e \dfrac{du_e}{dx}}{\dfrac{\tau_w}{\rho_e}}$$

The variation of χ along the nozzle with du_e/dx replaced by dv_e/dx is shown in Fig. 15 at T_t = 1500 °R for the range of stagnation pressures from 45 to 254 psia. With decreasing stagnation pressure, the increasing values of χ indicate the predicted reduced net production of turbulent kinetic energy. At the lowest stagnation pressure, χ attains a maximum value of about 0.25. Actually, for the low stagnation pressures, the values of χ should exceed those shown, since the low heat transfer implies that the wall shear is below the predicted value. The variation of χ along the nozzle displays the same trend of being largest in the convergent section before diminishing through the throat and divergent section as the departure of the heat-transfer data at the low stagnation pressures from that typical of a turbulent boundary layer observed in Fig. 9. The values of χ indicate when the turbulent shear stress, $\overline{u'v'}$, which is related to the turbulent kinetic energy, is expected to be lower than that typical of a fully turbulent boundary layer. The transport of heat would also be reduced, since it depends on the level of turbulent transport.

CONCLUSIONS

Experimental convective heat-transfer results have been presented for a turbulent boundary-layer flow through a cooled convergent-divergent nozzle. The scope of the investigation covered a wide range of stagnation pressures and temperatures as well as nozzle-inlet boundary-layer thicknesses. The experimental results indicated the following:

1. Heat-transfer coefficients increased with increasing stagnation pressure as a result of the larger mass fluxes, but only at stagnation pressures above about 75 psia were values typical of a turbulent boundary layer.

2. At low stagnation pressures, the heat-transfer coefficients were below that typical of a turbulent boundary layer even though the boundary layers at the nozzle inlet were turbulent.

3. The effect of stagnation temperature on heat transfer was less clear, with the trends dependent on stagnation pressure.

4. Heat-transfer coefficients were about 10% higher throughout the nozzle with the thinnest boundary layer at the nozzle inlet ($\delta/R \simeq 0.05$) than in the nozzle with the thickest inlet boundary layer ($\delta/R \simeq 0.25$).

5. The heat-transfer coefficient is a maximum upstream of the throat, where the mass flux, deduced from wall static pressure measurements, is largest. Deviations of the mass flux from that predicted for

one-dimensional flow amounted to as much as 15% just downstream of the throat.

6. A substantial decrease in heat transfer existed downstream of the point of flow separation. Flow separation in the divergent portion of the nozzle occurred at the low stagnation pressures.

Various heat-transfer predictions were compared to the data. Fair agreement at the higher stagnation pressures is provided by a modification of the turbulent boundary-layer analysis of Ref. 10, in which the Stanton number is taken dependent on a Reynolds number based on a thickness characteristic of the thermal boundary layer. In this prediction, properties were evaluated at the free-stream temperature. For the low stagnation pressures, where the turbulent boundary layer is thought to have undergone partial transition toward a laminar one, a parameter is found which is a measure of the importance of flow acceleration in reducing the transport of heat below that typical of a fully turbulent boundary layer.

More work is needed to gain some experimental knowledge of the flow and thermal boundary layers within a convergent-divergent nozzle and of the extent to which these are predictable by an analysis such as that of Ref. 11. To obtain this information, a conical nozzle of 10-deg half-angles of convergence and divergence has been constructed. This nozzle, which will be tested in the near future, is instrumented with boundary-layer probes and incorporates the calorimetric technique to obtain heat-transfer measurements.

REFERENCES

1. A. B. Witte and E. Y. Harper, Experimental Investigation and Empirical Correlation of Local Heat Transfer Rates in Rocket Engine Thrust Chambers, Technical Report 32-244, Jet Propulsion Laboratory, Pasadena, March 19, 1962.

2. O. A. Saunders and P. H. Calder, "Some Experiments on the Heat Transfer from a Gas Flowing Through a Convergent-Divergent Nozzle," Proceedings of the 1951 Heat Transfer and Fluid Mechanics Institute, Stanford University Press, 1951.

3. H. J. Kolozsi, An Investigation of Heat Transfer through the Turbulent Boundary Layer in an Axially Symmetric, Convergent-Divergent Nozzle, Aerodynamic Lab., Ohio State University, TM-8, July 1958.

4. W. C. Ragsdale and J. M. Smith, Heat transfer in nozzles, Chem. Engr. Sci., 11, 242, (1960).

5. Combined Bimonthly Summary No. 63, Dec. 1, 1957 to Feb. 1, 1958, Jet Propulsion Laboratory, Pasadena, pp. 28-30, Feb. 15, 1958. Combined Bimonthly Summary No. 65, April 1, 1958 to June 1, 1958, Jet Propulsion Laboratory, Pasadena, p. 32, June 15, 1958.

6. J. L. Livesey," The behavior of transverse cylindrical and forward facing pressure probes in transverse total pressure gradients,"Journal of the Aeronautical Sciences, 23, 949-955, (October 1956).

7. K. Oswatitsch and W. Rothstein, Flow Pattern in a Converging-Diverging Nozzle, NACA TM-1215, March 1949.

8. A. A. Sergienko and V. K. Gretsov,"Transition from a turbulent into a laminar boundary layer," Soviet Physics Doklady, 4, No. 2, 275-276, (October 1959).

9. L. H. Back, Heat Transfer to Turbulent Boundary Layers with a Variable Free-Stream Velocity, Ph.D. Thesis, University of California, Berkeley, California, June 1962.

10. D. R. Bartz,"An approximate solution of compressible turbulent boundary-layer development and convective heat transfer in convergent-divergent nozzles," Trans. ASME, 77, No. 8, 1235-1245, (1955).

11. D. G. Elliott, D. R. Bartz, S. Silver, Calculation of Turbulent Boundary-Layer Growth and Heat Transfer in Axi-Symmetric Nozzles, Technical Report No. 32-387, Jet Propulsion Laboratory, Pasadena, February 15, 1963.

12. R. A. Seban and H. W. Chan, Heat Transfer to Boundary Layers with Pressure Gradients, University of California, Institute of Engineering Research, Series 41, No. 1?, July 1957.

13. T. F. Mc Carthy, Heat Transfer to Turbulent Boundary Layers with a Pressure Gradient, Master's Thesis, University of Minnesota, August 1960.

14. D. E. Coles, The Turbulent Boundary Layer in a Compressible Fluid, Report No. P-2417, The Rand Corporation, Santa Monica, California, Aug. 22, 1961.

15. D. Wolf, "Heating and Cooling Air and Carbon Dioxide in the Thermal Entrance Region of a Circular Duct With Large Gas-to-Wall Temperature Differences," Transactions of the ASME Journal of Heat Transfer, 81, Series C, 267-279 (1959).

16. S. S. Kutateladze and A. I. Leontev, "Drag Law in a Turbulent Flow of a Compressible Gas and the Method of Calculating Friction and Heat Exchange," Akad. Nauk, Belorussk, S.S.R., Minsk, 1-23, 23-27 Jan. 1961, U.S.S.R.; Translated and issued by Technical Information and Library Services, Ministry of Aviation, Dec. 1961.

17. D. R. Bartz, "A simple equation for rapid estimation of rocket nozzle convective heat-transfer coefficients," Jet Propulsion, 27, 49-51 (Jan. 1957).

18. J. H. Preston, "The minimum Reynolds number for a turbulent boundary layer and the selection of a transition devices," Journal of Fluid Mechanics, 3, Part 4, 373-384 (Jan. 1958).

19. J. O. Hinze, Turbulence, p. 62, McGraw-Hill Book Company, Inc., New York, New York (1959).

20. P. S. Klebanoff, Characteristics of Turbulence in a Boundary Layer with Zero Pressure Gradient, NACA TN-3178, 1954.

LIST OF FIGURES

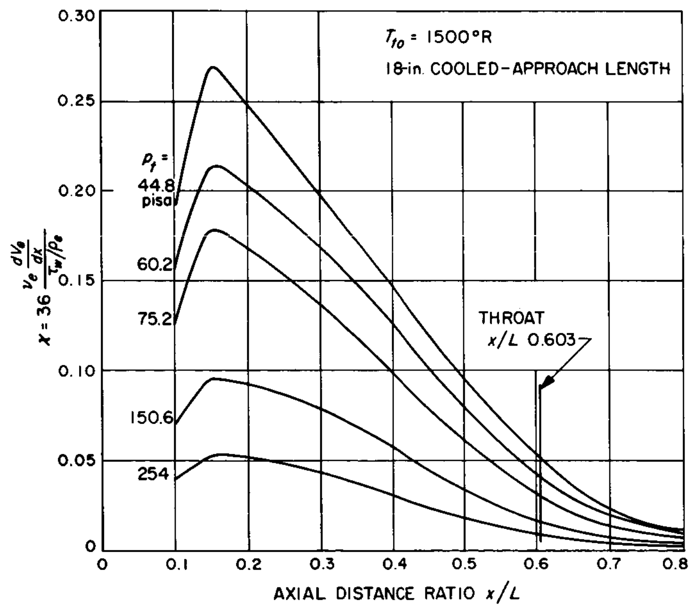

0.30
0.25
0.20
0.15
0.10
0.05
0
$\chi = 36 \frac{\nu_e \frac{dV_e}{dx}}{\tau_w/\rho_e}$
T_{t0} = 1500°R
18-in. COOLED-APPROACH LENGTH
p_t =
44.8
pisa
60.2
75.2
150.6
254
THROAT
x/L 0.603
0
0.1
0.2
0.3
0.4
0.5
0.6
0.7
0.8
AXIAL DISTANCE RATIO x/L

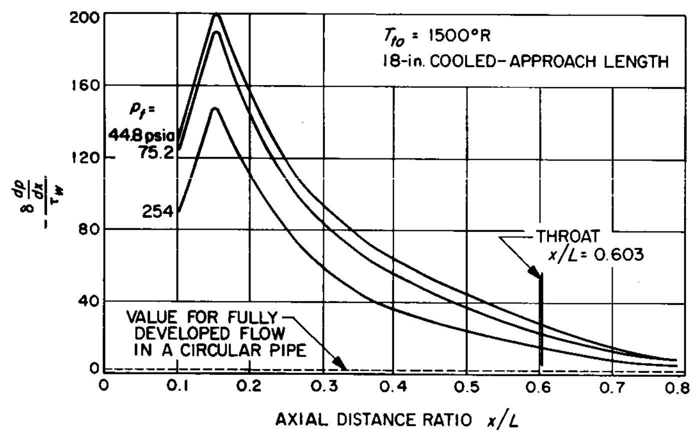

T_{t0} = 1500°R
18-in. COOLED-APPROACH LENGTH
p_t =
44.8 psia
75.2
254
THROAT
x/L = 0.603
VALUE FOR FULLY DEVELOPED FLOW IN A CIRCULAR PIPE
AXIAL DISTANCE RATIO x/L

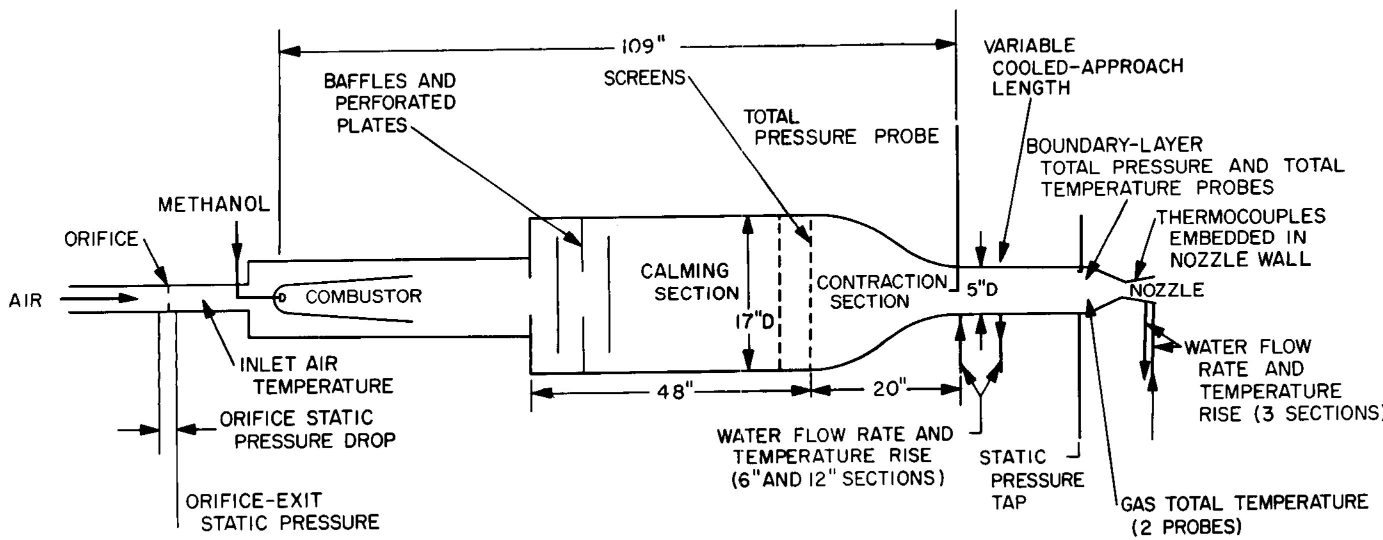
109"
VARIABLE COOLED-APPROACH LENGTH
BAFFLES AND PERFORATED PLATES
SCREENS
TOTAL PRESSURE PROBE
BOUNDARY-LAYER TOTAL PRESSURE AND TOTAL TEMPERATURE PROBES
THERMOCOUPLES EMBEDDED IN NOZZLE WALL
METHANOL
ORIFICE
AIR
COMBUSTOR
CALMING SECTION
17"D
CONTRACTION SECTION
5"D
NOZZLE
WATER FLOW RATE AND TEMPERATURE RISE (3 SECTIONS)
INLET AIR TEMPERATURE
48"
20"
ORIFICE STATIC PRESSURE DROP
WATER FLOW RATE AND TEMPERATURE RISE (6" AND 12" SECTIONS)
STATIC PRESSURE TAP
ORIFICE-EXIT STATIC PRESSURE
GAS TOTAL TEMPERATURE (2 PROBES)

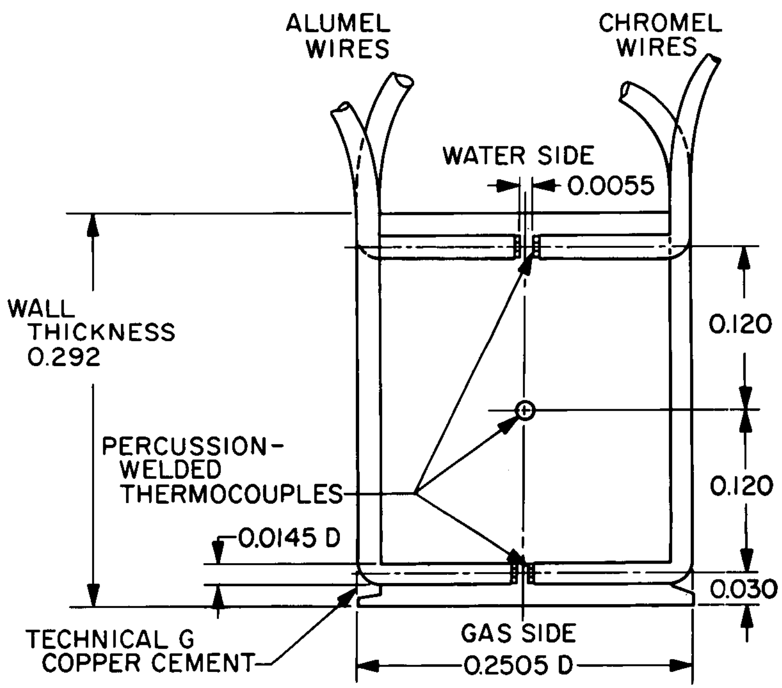

DIMENSIONS IN INCHES

PLUG No.	PLUG POSITION[a] x/L	A/A*	CIRCUMFERENTIAL ANGLE FROM ARBITRARY ZERO deg
I24	0.133	6.39	330
D25	0.204	5.05	30
D34	0.276	3.86	150
I23	0.336	2.98	280
D26	0.385	2.37	80
D35	0.429	1.88	200
I22	0.469	1.48	315
D28	0.512	1.23	45
H37[b]	0.541	1.10	155
I20[c]	0.573	1.02	300
D29	0.603	1.00	60
F42	0.634	1.02	180
I19	0.664	1.08	285
D30	0.693	1.19	75
F43	0.717	1.28	200
I18	0.750	1.41	320
D31	0.782	1.55	40
F45[c]	0.825	1.74	150
I17	0.864	1.94	275
C16	0.864	1.94	320
D33	0.905	2.14	85
F46	0.938	2.41	205

[a] $L = 5.925$ in. and $A^* = 2.552$ in.^{2} at $x/L = 0.603$.
[b] Data from this plug are questionable and have been omitted.
[c] Water side wall thermocouple in this plug has been damaged.

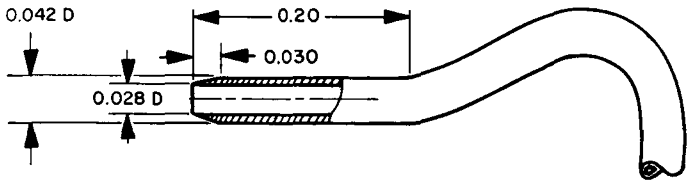

STAGNATION PRESSURE PROBE

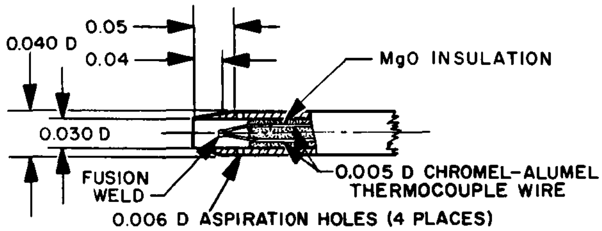

STAGNATION TEMPERATURE PROBE

DIMENSIONS IN INCHES

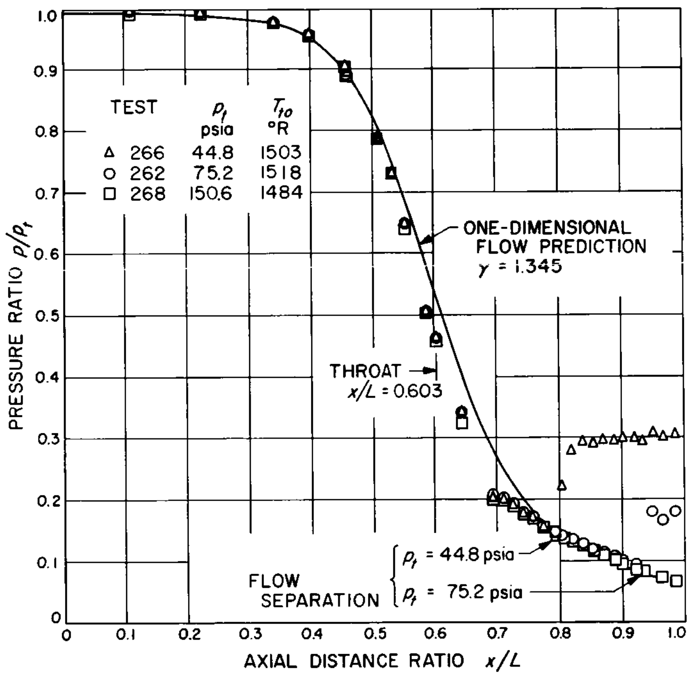
TEST
p_t psia
T_{to} °R
△ 266 44.8 1503
○ 262 75.2 1518
□ 268 150.6 1484
ONE-DIMENSIONAL FLOW PREDICTION
γ = 1.345
THROAT
x/L = 0.603
FLOW SEPARATION
p_t = 44.8 psia
p_t = 75.2 psia
PRESSURE RATIO p/p_t
AXIAL DISTANCE RATIO x/L
0
0.1
0.2
0.3
0.4
0.5
0.6
0.7
0.8
0.9
1.0

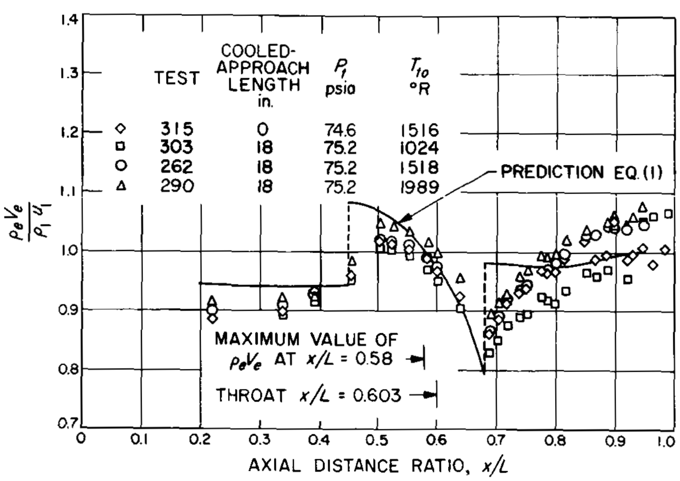
TEST
COOLED-APPROACH LENGTH in.
P_1 psia
T_{10} °R
315 0 74.6 1516
303 18 75.2 1024
262 18 75.2 1518
290 18 75.2 1989
PREDICTION EQ.(1)
MAXIMUM VALUE OF $\rho_e V_e$ AT x/L = 0.58
THROAT x/L = 0.603
$\frac{\rho_e V_e}{\rho_1 u_1}$
AXIAL DISTANCE RATIO, x/L

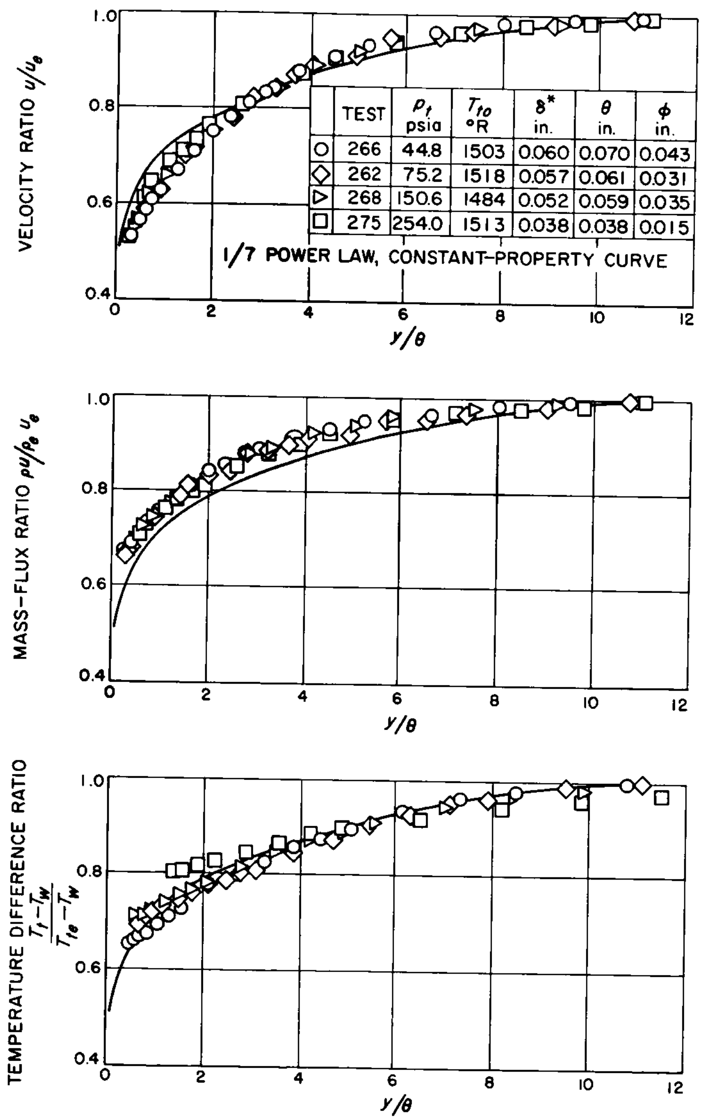

VELOCITY RATIO u/u_e
MASS-FLUX RATIO $\rho u/\rho_e u_e$
TEMPERATURE DIFFERENCE RATIO $\frac{T_t - T_w}{T_{te} - T_w}$
y/θ
1/7 POWER LAW, CONSTANT-PROPERTY CURVE

	TEST	p_t psia	T_{to} °R	δ^* in.	θ in.	ϕ in.
○	266	44.8	1503	0.060	0.070	0.043
◇	262	75.2	1518	0.057	0.061	0.031
▷	268	150.6	1484	0.052	0.059	0.035
□	275	254.0	1513	0.038	0.038	0.015

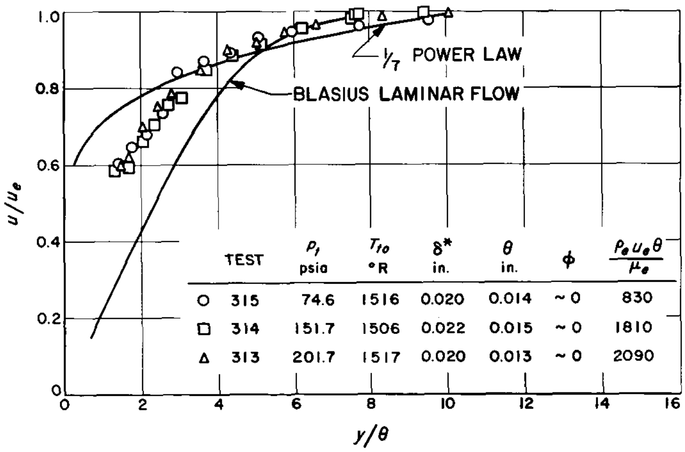
1.0
0.8
0.6
0.4
0.2
0
u/u_e
0
2
4
6
8
10
12
14
16
y/θ
1/7 POWER LAW
BLASIUS LAMINAR FLOW
TEST | p_t psia | T_to °R | δ* in. | θ in. | φ | ρ_e u_e θ / μ_e
○ 315 | 74.6 | 1516 | 0.020 | 0.014 | ~0 | 830
□ 314 | 151.7 | 1506 | 0.022 | 0.015 | ~0 | 1810
△ 313 | 201.7 | 1517 | 0.020 | 0.013 | ~0 | 2090

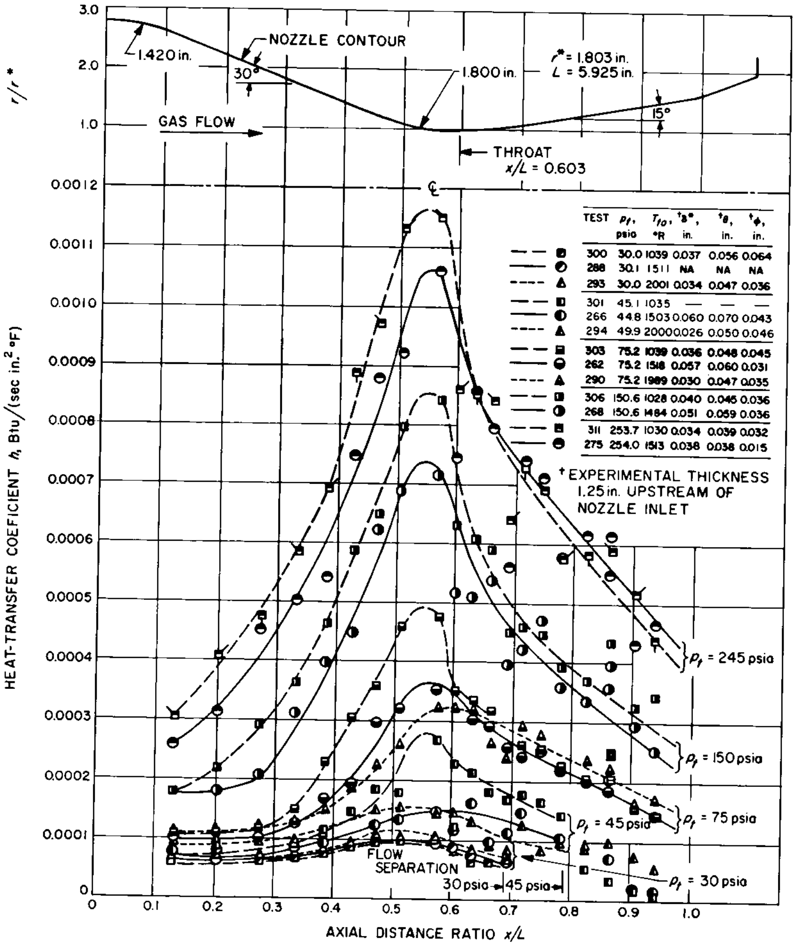

NOZZLE CONTOUR
1.420 in.
30°
1.800 in.
r^* = 1.803 in.
L = 5.925 in.
15°
GAS FLOW
THROAT
x/L = 0.603
r/r^*
TEST | p_t, psia | T_{t0}, °R | †δ*, in. | †θ, in. | †φ, in.
300 30.0 1039 0.037 0.056 0.064
288 30.1 1511 NA NA NA
293 30.0 2001 0.034 0.047 0.036
301 45.1 1035 — — —
266 44.8 1503 0.060 0.070 0.043
294 49.9 2000 0.026 0.050 0.046
303 75.2 1039 0.036 0.048 0.045
262 75.2 1518 0.057 0.060 0.031
290 75.2 1989 0.030 0.047 0.035
306 150.6 1028 0.040 0.045 0.036
268 150.6 1484 0.051 0.059 0.036
311 253.7 1030 0.034 0.039 0.032
275 254.0 1513 0.038 0.038 0.015
† EXPERIMENTAL THICKNESS 1.25 in. UPSTREAM OF NOZZLE INLET
p_t = 245 psia
p_t = 150 psia
p_t = 75 psia
p_t = 45 psia
p_t = 30 psia
FLOW SEPARATION
30 psia
45 psia
HEAT-TRANSFER COEFICIENT h, Btu/(sec in.^{2} °F)
AXIAL DISTANCE RATIO x/L

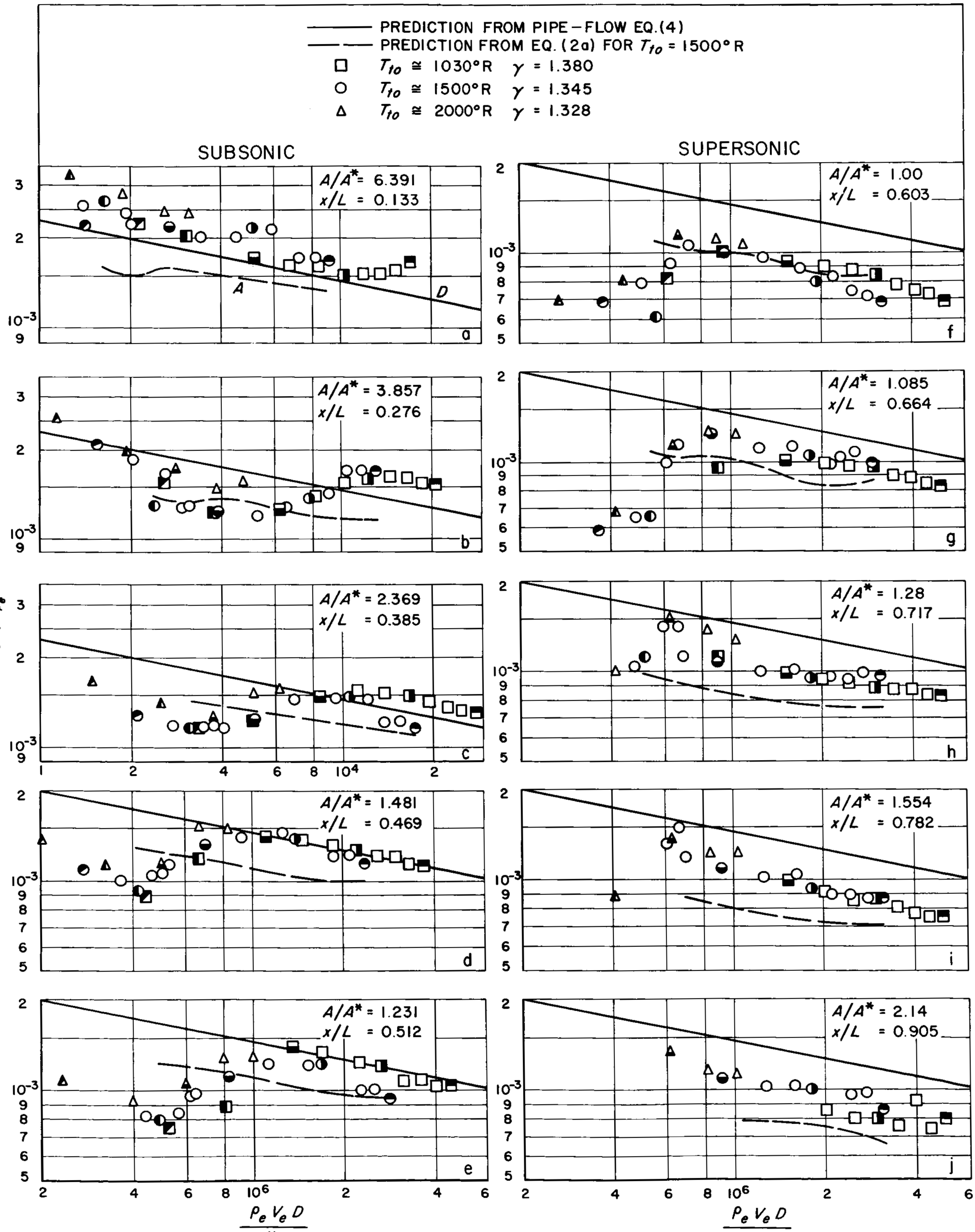

PREDICTION FROM PIPE-FLOW EQ.(4)
PREDICTION FROM EQ.(2a) FOR T_{to} = 1500°R
$T_{to} \cong$ 1030°R γ = 1.380
$T_{to} \cong$ 1500°R γ = 1.345
$T_{to} \cong$ 2000°R γ = 1.328
SUBSONIC
SUPERSONIC
A/A^* = 6.391 x/L = 0.133
A/A^* = 3.857 x/L = 0.276
A/A^* = 2.369 x/L = 0.385
A/A^* = 1.481 x/L = 0.469
A/A^* = 1.231 x/L = 0.512
A/A^* = 1.00 x/L = 0.603
A/A^* = 1.085 x/L = 0.664
A/A^* = 1.28 x/L = 0.717
A/A^* = 1.554 x/L = 0.782
A/A^* = 2.14 x/L = 0.905
$\frac{h}{\rho_e V_e C_{p_e}} Pr_e^{0.6}$
$\frac{\rho_e V_e D}{\mu_e}$

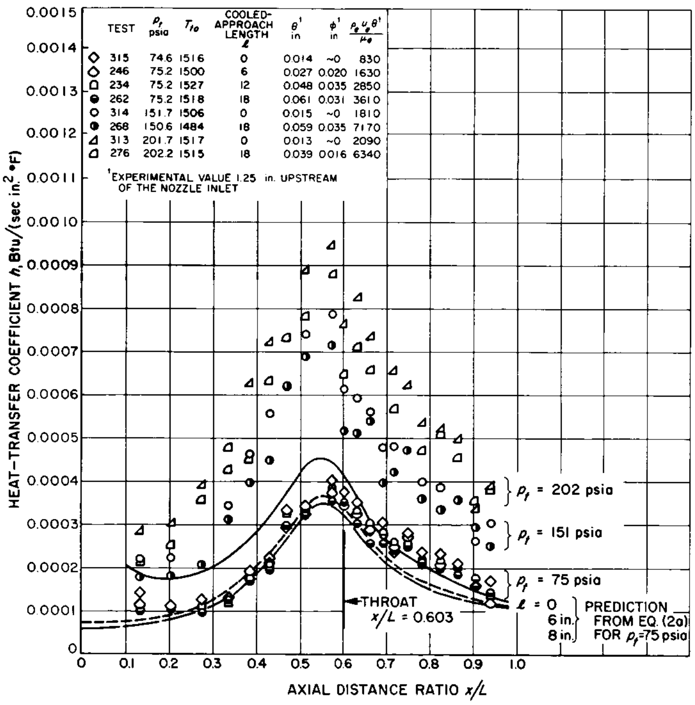

TEST p_t psia T_{t0} COOLED-APPROACH LENGTH ℓ θ^1 in ϕ^1 in $\frac{\rho_e u_e \theta^1}{\mu_e}$
315 74.6 1516 0 0.014 ~0 830
246 75.2 1500 6 0.027 0.020 1630
234 75.2 1527 12 0.048 0.035 2850
262 75.2 1518 18 0.061 0.031 3610
314 151.7 1506 0 0.015 ~0 1810
268 150.6 1484 18 0.059 0.035 7170
313 201.7 1517 0 0.013 ~0 2090
276 202.2 1515 18 0.039 0.016 6340
[1]EXPERIMENTAL VALUE 1.25 in. UPSTREAM OF THE NOZZLE INLET
HEAT-TRANSFER COEFFICIENT h, Btu/(sec in.^{2} °F)
AXIAL DISTANCE RATIO x/L
THROAT x/L = 0.603
p_t = 202 psia
p_t = 151 psia
p_t = 75 psia
ℓ = 0, 6 in., 8 in. PREDICTION FROM EQ. (2a) FOR p_t=75 psia

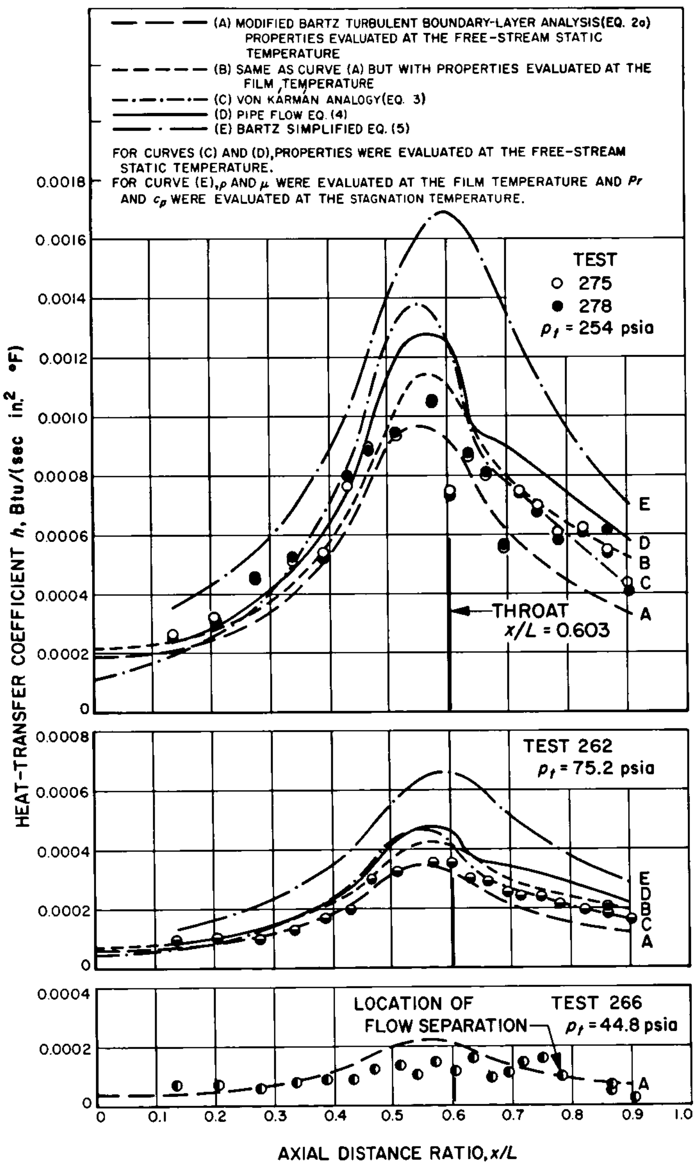

(A) MODIFIED BARTZ TURBULENT BOUNDARY-LAYER ANALYSIS (EQ. 2a) PROPERTIES EVALUATED AT THE FREE-STREAM STATIC TEMPERATURE
(B) SAME AS CURVE (A) BUT WITH PROPERTIES EVALUATED AT THE FILM TEMPERATURE
(C) VON KÁRMÁN ANALOGY (EQ. 3)
(D) PIPE FLOW EQ. (4)
(E) BARTZ SIMPLIFIED EQ. (5)
FOR CURVES (C) AND (D), PROPERTIES WERE EVALUATED AT THE FREE-STREAM STATIC TEMPERATURE.
FOR CURVE (E), ρ AND μ WERE EVALUATED AT THE FILM TEMPERATURE AND Pr AND c_p WERE EVALUATED AT THE STAGNATION TEMPERATURE.
TEST
275
278
p_t = 254 psia
THROAT
x/L = 0.603
TEST 262
p_t = 75.2 psia
LOCATION OF FLOW SEPARATION
TEST 266
p_t = 44.8 psia
E
D
B
C
A
HEAT-TRANSFER COEFFICIENT h, Btu/(sec in.² °F)
AXIAL DISTANCE RATIO, x/L

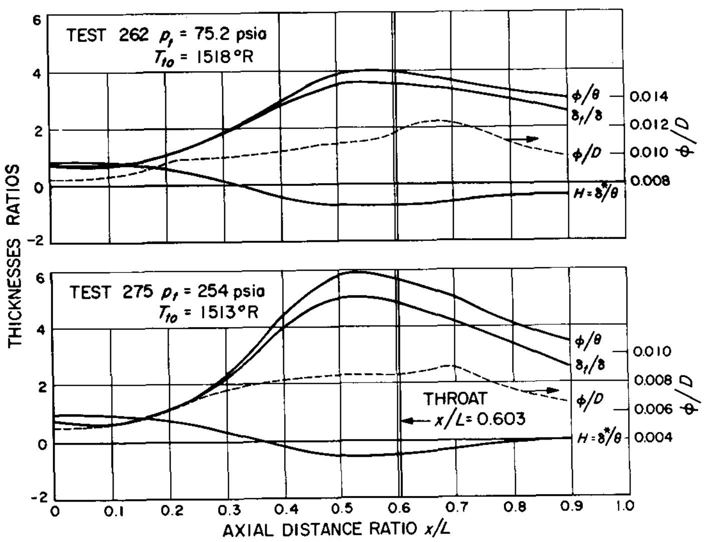

TEST 262 p_t = 75.2 psia
T_{to} = 1518°R
TEST 275 p_t = 254 psia
T_{to} = 1513°R
THROAT
x/L = 0.603
ϕ/θ
δ_1/δ
ϕ/D
$H = \delta^*/\theta$
THICKNESSES RATIOS
AXIAL DISTANCE RATIO x/L
ϕ/D
ϕ/D

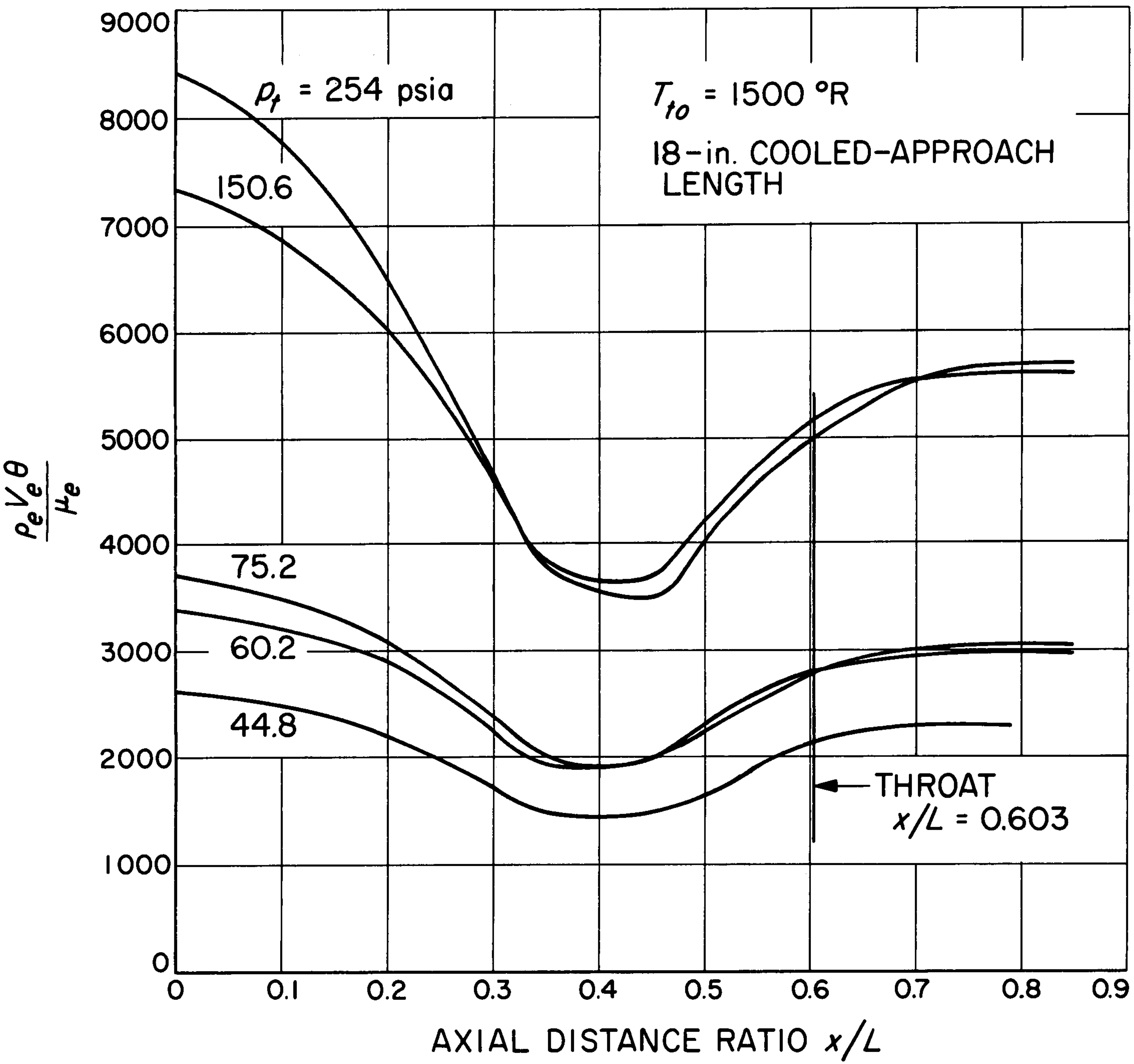

p_t = 254 psia
150.6
75.2
60.2
44.8
T_{to} = 1500 °R
18-in. COOLED-APPROACH LENGTH
THROAT x/L = 0.603
$\frac{\rho_e V_e \theta}{\mu_e}$
9000
8000
7000
6000
5000
4000
3000
2000
1000
0
0.1
0.2
0.3
0.4
0.5
0.6
0.7
0.8
0.9
AXIAL DISTANCE RATIO x/L